A roadmap for poly(ethylene oxide)-block-poly-ε-caprolactone self-assembly in water : prediction, synthesis, and characterization and characterization

A Roadmap for Poly(ethylene oxide)-*block*-Poly-ε-caprolactone Self-Assembly in Water: Prediction, Synthesis, and Characterization

Alessandro Ianiro,[1,2] Joseph Patterson,[2,3] Álvaro González García,[1,4] Mark M. J. van Rijt,[2,3] Marco M. R. M Hendrix,[1,2] Nico A. J. M. Sommerdijk,[2,3] Ilja K. Voets,[1,2,5] A. Catarina C. Esteves,[1] Remco Tuinier [1,2,4]

[1]Laboratory of Physical Chemistry, Department of Chemical Engineering and Chemistry, Eindhoven University of Technology, MB 5600, Eindhoven, The Netherlands
[2]Institute for Complex Molecular Systems, Eindhoven University of Technology, P.O. Box 513, MB 5600, Eindhoven, The Netherlands
[3]Laboratory of Materials and Interface Chemistry and Centre for Multiscale Electron Microscopy Department of Chemical Engineering and Chemistry, Eindhoven University of Technology, P.O. Box 513, MB 5600, Eindhoven, The Netherlands
[4]Van't Hoff Laboratory for Physical and Colloid Chemistry, Department of Chemistry and Debye Institute, Utrecht University, Padualaan 8, CH 3584, Utrecht, The Netherlands
[5]Laboratory for Macromolecular and Organic Chemistry, Department of Chemical Engineering and Chemistry, Eindhoven University of Technology, P.O. Box 513, MB 5600, Eindhoven, The Netherlands
Correspondence to: R. Tuinier (E-mail: r.tuinier@tue.nl)

Received 19 July 2017; accepted 27 October 2017; published online 14 November 2017
DOI: 10.1002/polb.24545

ABSTRACT: Numerical self-consistent field (SCF) lattice computations allow *a priori* determination of the equilibrium morphology and size of supramolecular structures originating from the self-assembly of neutral block copolymers in selective solvents. The self-assembly behavior of poly(ethylene oxide)-*block*-poly-ε-caprolactone (PEO-PCL) block copolymers in water was studied as a function of the block composition, resulting in equilibrium structure and size diagrams. Guided by the theoretical SCF predictions, PEO-PCL block copolymers of various compositions have been synthesized and assembled in water. The size and morphology of the resulting structures have been characterized by small-angle X-ray scattering, cryogenic transmission electron microscopy, and multiangle dynamic light scattering. The experimental results are consistent with the SCF computations. These findings show that SCF is applicable to build up roadmaps for amphiphilic polymers in solution, where control over size and shape are required, which is relevant, for instance, when designing spherical micelles for drug delivery systems © 2017 Wiley Periodicals, Inc. J. Polym. Sci., Part B: Polym. Phys. **2018**, *56*, 330–339

KEYWORDS: block copolymers; drug delivery; modeling; phase diagrams; self-assembly

INTRODUCTION Amphiphilic block copolymers have been given great attention due to their ability to assemble into well-defined supramolecular architectures. In selective solvents the lyophobic blocks associate to minimize their interface with the solvent, while the lyophilic blocks remain solvated. This results in the formation of structures where the blocks are segregated in two regions, a dense desolvated core composed of the collapsed lyophobic chains and a swollen solvated corona surrounding the core.[1,2] Depending on composition, chain lengths of the blocks, and the self-assembly process, architectures with different size and morphologies can be obtained.[3–5] These structures find applications in many advanced scientific and industrial fields.[5–10]

The ability to relate the copolymer composition to the self-assembly behavior, to finely control morphology and size is a central theme in the development of block copolymer self-assembly field. This is most commonly done by experimental trial and error, which has two main drawbacks: first, it represents a high investment of time and resources; second, the features of the self-assembled structures can strongly depend on the adopted preparation procedure.[11] The latter is related to the fact that block copolymer assemblies can get stuck in kinetic traps, which may remain stable in solution for long periods[12,13] or continually evolve over time.[11] However, it is difficult to predict and control the self-assembly of kinetically trapped structures, which can lead to

This article was published online on 14 November 2017. After online publication, an incorrect Orcid ID was removed from one of the authors. This notice is included in the online and print versions to indicate that both have been corrected on 1 December 2017.

Additional Supporting Information may be found in the online version of this article.

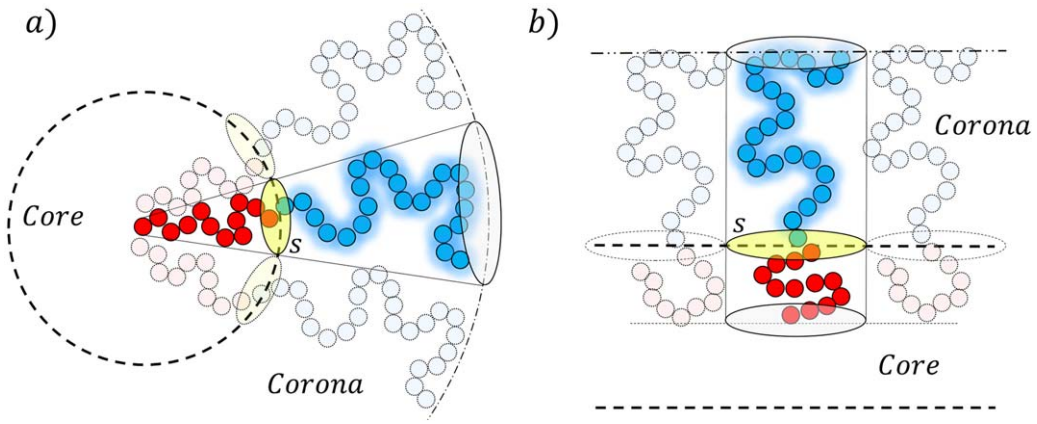

FIGURE 1 Schematic representation of a block copolymer in a spherical micelle (a) and a flat bilayer (b). The interfacial area of the chains is noted in yellow. [Color figure can be viewed at wileyonlinelibrary.com]

even more exhaustive trial-and-error based approaches. A solution to avoid the drawback of the experimental investigations is to rely on a theoretical method which enables quantitative prediction of the desired equilibrium morphology and size, and then to use experimental approaches to obtain these equilibrium structures in solution.

To explain why different copolymers adopt different architectures the packing parameter P[14] is frequently used. The quantity P is defined as V/sL, where V is the volume of the lyophobic block, L is length, and s the specific area occupied by one copolymer molecule at the core corona interface. However, it is not possible to directly relate block copolymer architecture to P, since the estimation of s and V requires the knowledge of the aggregation number, the core size, and the solvent volume fraction inside the micelle. These values must be provided via experimental or computational methods.

Analytical theories have been developed to describe the self-association of block copolymers.[15–17] The predictive power of such theories is, however, limited. For example, the scaling models proposed by Zhulina et al. and Zhulina and Borisov[15,17] can give reliable predictions regarding size and aggregation number for spherical micelles, but for other morphologies they can only describe the scaling behavior.[17]

Full computer simulation methods such as molecular dynamics (MD) can provide precise information about the self-assembly behavior of block copolymers. However, the high computational cost of such methods does not allow systematic investigations on practical timescales. A powerful tool to obtain reliable thermodynamic and structural information, and predict the size and morphology of self-assembled architectures is the Scheutjens-Fleer self-consistent field (SCF) theory.[1,18] In this model, the polymers and the solvent are distributed over a lattice. The conformational space of the molecules is explored via a step-weighted random walk to calculate the conformational entropy, while the enthalpy of the self-assembly process is modeled via a set of pair interaction parameters, also called Flory-Huggins or χ parameters. The χ parameters describe the enthalpy variation upon contact between a pair of components of the system, and can be estimated theoretically or measured experimentally.[19,20] A mean-field approximation and full occupancy of the lattice (no vacuum sites in the lattice) are assumed.[1,18,21] Due to the low computational cost (typically at least 10^4 times faster than full computer simulations), SCF calculations provide a fast and effective way to perform systematic investigations. When the χ parameters are accurate and the coarse-graining of the copolymers reflects the flexibility of the blocks, the SCF computations can give quantitatively accurate predictions.

In selective solvents, amphiphilic macromolecules tend to arrange in such a way that the interfacial area s (Fig. 1) between the lyophobic block and solvent is minimized. As the chains get closer, upon an increase in the aggregation number g, they start to feel each other's steric repulsion. To reduce this repulsion, the chains stretch toward the solvent, resulting in an increase in the corona thickness (Fig. 1). This stretching is unfavorable, acting as a stopping mechanism for the growth of the micelle.[22]

The steric repulsions between the lyophilic chains are affected by the curvature of the interface between core and corona. In particular, a higher curvature leads to larger space available for the lyophilic chains. Therefore, the steric repulsion is relatively small in spherical morphologies [Fig. 1(a)] and large for flat morphologies [Fig. 1(b)]. The lyophobic chains in the core also experience stretching, related to the curvature of the interface, but in an opposite fashion. Getting closer to the center of the core, the chains have less space available if the curvature of the interface is high. Therefore, the lyophobic chains will stretch more in the spherical geometry [Fig. 1(a)] than in the flat one [Fig. 1(b)]. The balance of three contributions: (i) reduction in the interfacial energy, (ii) chain stretching in the coron, and (iii) chain stretching in the core, determines the equilibrium morphology, characteristic size, and aggregation number of the self-assembled structure.[17]

As this balance is complex and cannot be expressed in the form of an exact analytical solution, an approximate numerical

approach, such as the SCF method (see Supporting Information for more details), is required to compute the equilibrium properties of block copolymer self-assembled architectures.

In this work, we used the SCF method to systematically investigate the self-assembly behavior of poly(ethylene oxide)-*block*-poly-ε-caprolactone (PEO-PCL) block copolymers in water as a function of the length of the two blocks. The results of the computations have been used to build an equilibrium structure phase diagram and example concentration profiles for each morphology. The concentration profiles show how the volume fraction (ϕ) of each component varies as a function of the distance from the center (r) of the self-organized structure.

Building a predictive framework for PEO-PCL copolymers is important in virtue of their great potential in the biomedical field.[6,23] These copolymers are easy to prepare from cheap precursors, and the available synthetic methods allow high control over composition and molar mass dispersity.[24,25] Drug delivery and biomedical imaging are among the most promising fields where PEO-PCL copolymers are allowed by regulation.[26] PEO-PCL self-assembled structures in water are characterized by an insoluble core composed of the hydrophobic PCL block, suitable for the encapsulation of hydrophobic compounds,[27,28] such as drugs, dyes, and vitamins. The core is surrounded by a stabilizing PEO corona, which confers stealth properties to the structure, improving the cellular uptake.[29] For these applications, in particular, a high level of control over shape and dimension of the self-assembled structures is required. For example, recently, it has been shown how architectures with different morphologies possess different utility in biology and nanomedicine.[30–32]

Many experimental and theoretical investigations about the self-assembly behavior of PEO-PCL and other PEO-based block copolymers have been performed in an attempt to relate (block) copolymer composition[24,33–38] and chain rigidity[39–41] with the self-assembly behavior. It appears that given the multiplicity of factors affecting block copolymers self-assembly (blocks solubility, chain length, chain rigidity, and eventually specific interactions like hydrogen bonding), the construction of predictive self-assembly phase diagrams of such compounds needs to be performed on a case-by-case basis for each specific copolymer. Furthermore, for PEO-PCL, it is also clear that the preparation procedure has a drastic effect on the final morphology and size of the self-assembled aggregates of these copolymers, as discussed by Konishcheva et al. in a recent aricle.[42] It will be shown that the outcome of our SCF computations can provide useful insights to understand these results, in particular to understand weather a structure is at thermodynamic equilibrium or not. This information is important, as non-equilibrium structures can be characterized by a low colloidal stability and the tendency to evolve over time into more stable morphologies.

Finally, following the results provided by our SCF computations, we synthesized a set of PEO-PCL copolymers and experimentally explored their self-assembly behavior by small-angle X-ray scattering (SAXS), cryo-transmission electron microscopy (cryo-TEM), and multiangle dynamic light scattering (MA-DLS). The experimental results are consistent with our predictions. This demonstrates the potential of our predict–synthesize–characterize framework, which can be further applied to many other copolymer–solvent systems. Furthermore, it facilitates the design of polymer assemblies with specific characteristics which will enable efficient strategies for the end-use of such polymers, for example, encapsulation of hydrophobic compounds into PEO-PCL block copolymers.

MATERIALS AND METHODS

SCF Computations

The computations have been performed on lattices of three different geometries, spherical, cylindrical, and flat. In each lattice, gradients are accounted for in only one direction. In the spherical geometry, this provide a full description of the system. In the cylindrical geometry, the gradient follows the direction perpendicular to the length of the cylinder. In the flat geometry, it is perpendicular to the plane. Each lattice consist of 100 lattice layers in the direction of the gradient. The lattice size has been chosen such that a 50% decrease or a 50% increase in the number of layers does not affect the results of the computations. A coordination number of the lattice $z = 3$ was used for all the geometries. In the flat geometry, two mirrors are placed at the first and the last lattice sites to ensure periodic boundaries conditions. For spherical and cylindrical geometries, a mirror was located at the last lattice layer and the first layer corresponds to the center of the lattice. In the lattice, each solvent molecule (W) and ethylene oxide (A) monomer occupy one site, while caprolactone (B) monomer occupies two lattice sites. This is based on the fact that CL monomers have a molar mass and a molar volume which are roughly twice as large as that of EO. For example, a copolymer with the formula Me-EO_{45}-CL_{16} is modeled as A_{45}-B_{32} with equal size of the lattice sites for A and B. For all computations, the values $\chi_{WA}=0.4$, $\chi_{WB}=3$, and $\chi_{AB}=1$, reported by Lebouille et al.[43] have been used. It has been shown that these parameters well describe the PEO-PCL-Water system. The value of $\chi_{AB}=1$ has been chosen to account for water hydrogen-bonding to the PEO chains.[44,45] This mediates the interaction between the blocks and results in a high incompatibility.[46] Each lattice site was set to the size of an EO monomer (λ = 0.4 nm). This value was estimated by applying the relation

$\lambda=\left(\frac{M_{PEO}}{\rho \cdot n_{PEO} \cdot N_{AV}}\right)^{\frac{1}{3}}$, where λ is the lattice size, M_{PEO} is the molar mass of the PEO block, n_{PEO} its degree of polymerization, ρ its density, and N_{AV} the Avogadro's number.

All the copolymers in the computations are modeled as monodisperse. The synthesized polymers are modeled using their number averaged molar mass obtained by NMR (M_n^{NMR}) analyses (Table 1). The equilibrium morphology and the aggregation numbers have been computed according to the method described in the Supporting Information (particularly eqs S12 and S13) for copolymers composed of four

TABLE 1 Characteristics of the PEO-PCL Diblocks Synthesized in This Study

Copolymer	M_n^{NMR}(kDa)[a]	$Đ$[b]	Shape[c]	SCF Core (nm)[d]	SCF (nm)[e]	MA-DLS (nm)[f]	SAXS (nm)[g]	Cryo-TEM (nm)[h]
Me-EO_{45}-b-CL_{12}	3.3	1.08	S	4.5	9[i]	9 ± 1[i]	11 ± 1[i]	4 ± 2[i]
Me-EO_{45}-b-CL_{35}	6.0	1.34	C	7	12[j]	–	6 ± 1[j]	8 ± 4[j]
Me-EO_{45}-b-CL_{87}	12.0	1.28	B	16	28[k]	–	12 ± 1[k]	14 ± 9[k]

[a] Number-averaged molar mass (from NMR).
[b] Molar mass dispersity.
[c] Morphology of the self-assembled structure in water at $T = 295$ K: S = spherical, C = cylindrical, B = bilayer.
[d] Size of the PCL core obtained by SCF.
[e] Total hydrodynamic size from SCF.
[f] Size measured by MA-DLS.
[g] Size measured by SAXS.
[h] Size measured by cryo-TEM. Experimental size data are provided with the respective standard deviation.
[i] Value refers to the radius of spherical micelle R.
[j] Value refers to the cylindrical micelle cross sectional radius P.
[k] Value refers to the bilayers thickness H.

different PEO blocks ($n = 17$, $n = 30$, $n = 38$, $n = 45$).The PCL block length (m) was varied from 2 to 100 with a step size of 2 monomeric units (4 lattice units). The obtained SCF results were used to build an equilibrium structure diagram.

The equilibrium concentration profiles have been used to calculate the hydrodynamic radius (R_H), according to the method proposed by Scheutjens et al.[47] based on the Debye-Bueche equation for permeability (See Supporting Information for details about the procedure). The resulting R_H values have been used to construct size prediction diagrams.

Materials

Me-EO_{45} and ε-caprolactone (ε-CL) where purchased from Sigma Aldrich, fumaric acid (FA) from Fluka, and absolute ethanol and acetone from Biosolve, the Netherlands.

Synthesis and Purification of the Copolymers

Three different PEO-PCL copolymers, namely Me-EO_{45}-b-CL_{12}, Me-EO_{45}-b-CL_{35}, and Me-EO_{45}-b-CL_{87} have been synthesized and purified, using a one-pot metal-free ring opening polymerization procedure and a new purification method, respectively, as reported previously.[25]

The number-averaged molar mass M_n^{NMR} of the synthesized copolymers was calculated by ^{1}H NMR, carried out on a Varian 400 (400 MHz) spectrometer at 25 °C in deuterated chloroform. The molar mass dispersity $Đ = M_w/M_n$, were M_w is the weight-averaged molar mass, was determined from the molar mass distribution obtained by means of size exclusion chromatography (SEC), using a Waters GPC equipped with Waters (model 510) pump and a (model 410) differential refractometer. A set of two mixed bed columns (Mixed-C, Polymer Laboratories, 30 cm, 40 °C) was used and THF was selected as eluent. The system was calibrated using narrow molar mass polystyrene standards, ranging from 600 to 7106 Da.

Experimental Design: Preparation Procedure of Self-Assembled Structures

It has been shown that copolymer assemblies can be dynamic, that is, there is an exchange equilibrium between assembled and unassembled macromolecules.[48–50] Due to this exchange out of equilibrium structures can evolve toward the thermodynamic equilibrium. If the solubility of the copolymer is very low, this evolution becomes so slow that the structures can be considered as frozen.[50] Hence, in the experimental design, it is extremely important to select a preparation procedure which ensures the formation of assemblies close to the thermodynamic equilibrium. For PEO-PCL copolymers, it has been shown experimentally[37,42] (see Supporting Information Fig. S8 for a visual comparison) that the final morphology can be dependent on the preparation procedure, leading to the coexistence of mesoscale and nanoscale aggregates of various morphologies.

The preparation process plays an important role, especially for objects with complex geometry as cylinders or hollow spheres. Two different kinds of approaches are usually followed to prepare self-assembled structures: *bottom-up*, when the polymer is molecularly dissolved in a good solvent and forced to assemble by a solvent switch,[42] and *top-down*, where a precursor phase is induced to rearrange in solution.[51]

To prepare complex architectures with a *bottom-up* approach (e.g., solvent switch[42]), the chains need time to organize into a stable conformation. If the solvent switch is too fast, the lyophobic chains tend to collapse forming spherical objects, as this is a faster way to reduce their interfacial area. These structures are metastable and are not the most stable conformation that the system can adopt.[13]

To prepare structures close to equilibrium via a *top-down* approach (e.g., thin film rehydration[37,42]), three conditions need to be fulfilled: first, the chains need enough mobility to rearrange, meaning that the lyophobic blocks need to be above the glass transition temperature; second, the reorganization must lead to the segregation of lyophilic and lyophobic chains into two domains. This segregation needs a driving force. Such a driving force may consist of the intrinsic incompatibility between the two blocks together with the tendency of the hydrophilic block to maximize contact with the solvent. Third, the assemblies must be dynamic to reach the equilibrium value of g. In the case of PEO-PCL in solution

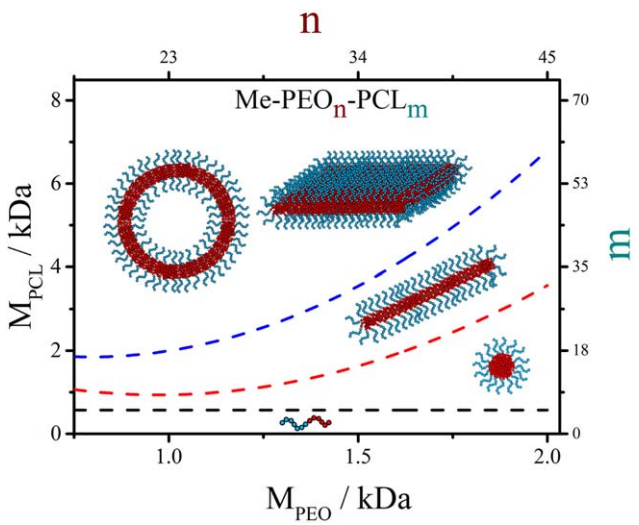

FIGURE 2 Morphology phase diagram for PEO-PCL block copolymers in water at $T = 20$ °C obtained by SCF. The dashed curves separate the stability regions for different morphologies. The composition of the copolymers are expressed in terms of mass (M) and block lengths (n and m). The region below the black dashed line indicates when the copolymer is soluble. The region between the black and the red dashed curve indicates the stability region for spherical micelles. The region between the red and the blue dashed curve cylindrical micelles is stable. The region above the blue dashed curve corresponds to the formation of vesicles or flat bilayers. [Color figure can be viewed at wileyonlinelibrary.com]

at room temperature, the presence of hydrogen-bonded water on the PEO chains[44,45] mediates the interaction between the blocks, resulting in a high effective incompatibility.[46] When the system is heated to promote film rehydration (see the preparation procedure adopted by Qi et al.[37]), the PCL chains gain mobility, but the PEO chains start to lose the hydrogen-bonded water and become insoluble. As a consequence, the stabilizing effect of the PEO domains and the overall copolymer solubility are strongly reduced. This may result in the formation of out of equilibrium structures.

One can deduce that a *bottom-up* approach should be preferred for copolymers with highly lyophobic blocks or thermosensitive lyophilic blocks. A *top-down* approach can be suitable for copolymers made of highly incompatible blocks with low glass transition temperature and relatively high solubility.

Our SCF model defines the equilibrium morphology and size of self-assembled structures as function of the copolymer composition (Figs. 2 and 3). If the parameters used for the modeling are accurate, a comparison between experimental results and SCF computations can be used as a feedback loop to rationalize whether or not a certain procedure results in the formation of equilibrium self-assembled structures.

Preparation of the Self-Assembled Structures

Depending on the expected morphology, two different procedures have been applied to prepare the self-assembled structures. For PEO-PCL spherical micelles, it has been shown that after a fast solvent switch, the formed structures are close to the thermodynamic equilibrium.[27,43] Thus, for the copolymer Me-EO$_{45}$-b-CL$_{12}$, that according to our model should assemble into spherical particles, the nanoprecipitation method,[52] consisting of an instantaneous solvent switch, was used. A solution has been prepared dissolving 20 mg of Me-EO$_{45}$-b-CL$_{12}$ in 1 mL of acetone. Each solution was then filtered with a 0.22 μm PTFE syringe filter, and 1 mL of the filtrate was quickly added to 9 mL of filtered deionized water. The solution was shaken by hand to ensure complete mixing. Other solutions have been prepared and analyzed via MA-DLS to investigate the effect of the starting concentration on the final features of the assemblies. Details of this analysis are reported in Supporting Information.

For polymers with long PCL blocks, such as Me-EO$_{45}$-b-CL$_{35}$ and Me-EO$_{45}$-b-CL$_{87}$, a fast solvent switch could result in the formation of kinetic aggregates. To avoid this, their self-assembly were prepared via a slow solvent switch. First, 1 mL of a 50-mg·mL^{-1} solution of each polymer, previously filtered with a 0.22-μm PTFE syringe filter, was placed in a clean 20 mL vial with magnetic stirring bar. Subsequently, 9 mL of water was slowly added by means of a syringe pump at the speed of 0.05 mL·min^{-1} under vigorous stirring. The vial was capped to avoid acetone evaporation and the water addition was performed through a hole in the cap via a Teflon capillary.

Characterization of the Self-Assembled Structures

A detailed description of the techniques and procedures used for the characterization of the self-assembled structures is reported in the Supporting Information.

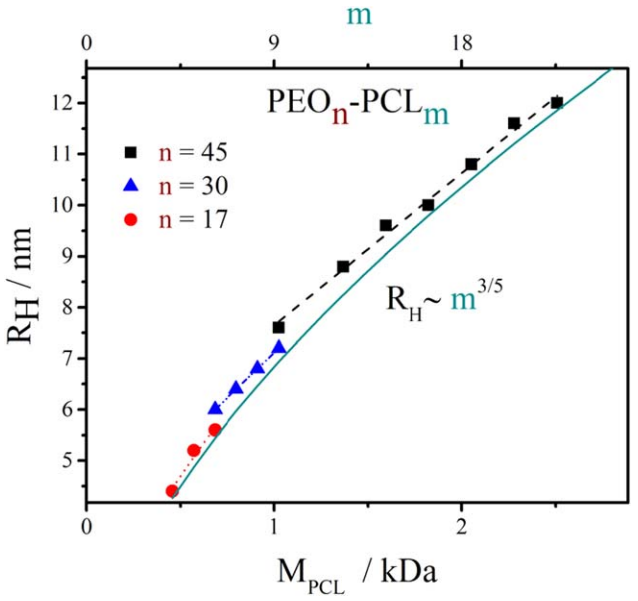

FIGURE 3 SCF size prediction diagram for Me-PEO-b-PCL copolymers of different compositions. Data points from SCF are compared with the scaling behavior predicted for star-like micelles by Zhulina and Borisov.[17] [Color figure can be viewed at wileyonlinelibrary.com]

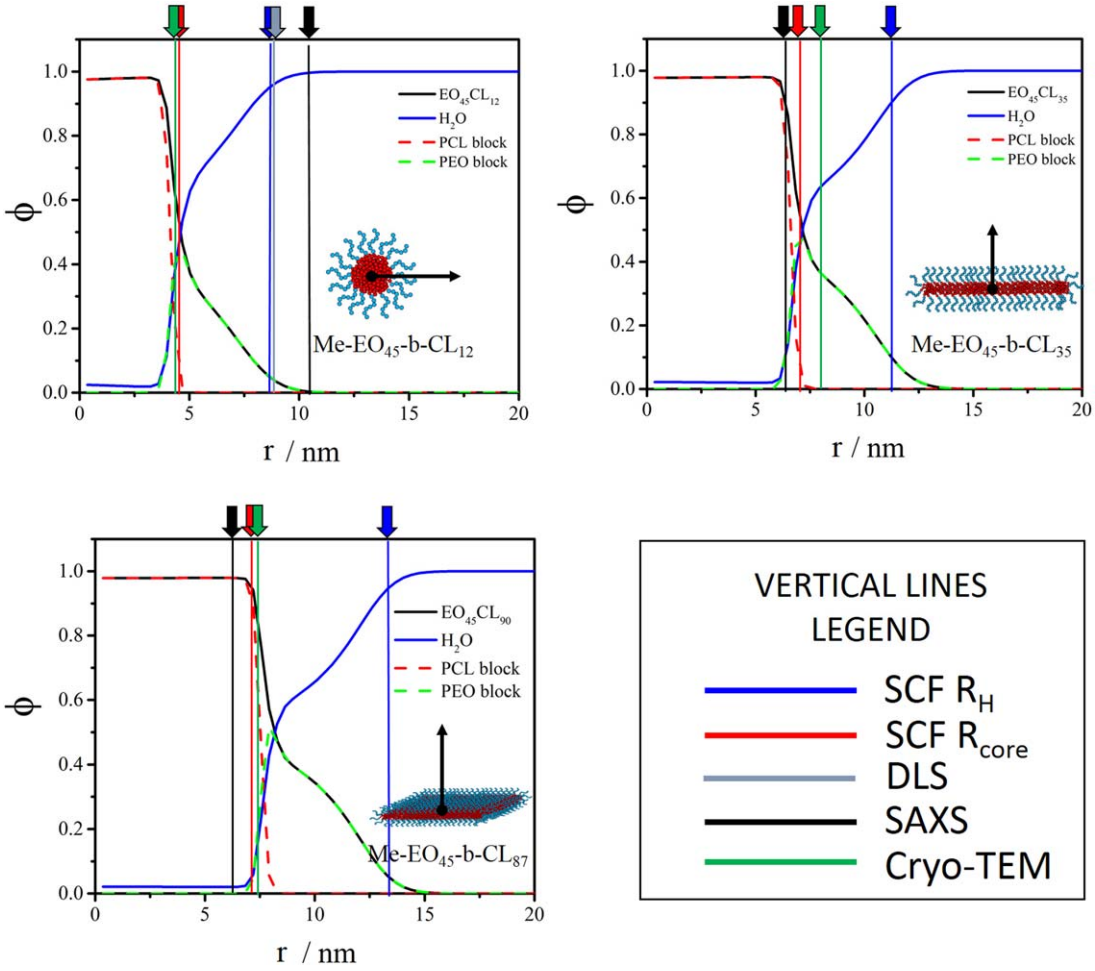

FIGURE 4 SCF concentration profiles for the self-assembled structures of some of the synthesized copolymers. The plots show how the volume fraction (ϕ) of a certain component changes as function of the distance from the center (r) of the structure. Predicted and experimentally measured sizes are depicted as vertical lines of different colors. [Color figure can be viewed at wileyonlinelibrary.com]

RESULTS AND DISCUSSION

Morphology, Size, and Radial Concentration Diagrams

The SCF computations for the PEO-PCL copolymers are summarized into an equilibrium structure phase diagram (Fig. 2), a size prediction diagram for spherical micelles (Fig. 3) and representative concentration profiles for the three different morphologies (spheres, cylinder, and bilayers) are plotted in Figure 4. The equilibrium structure phase diagram (Fig. 2) shows that as the relative mass of the PCL block increases with respect to the PEO block, the preferred morphology shifts from spheres, to cylinders, to bilayers. From the phase diagram, it appears that the change in morphology does not occur at a fixed PCL/PEO mass ratio, as the regions for the different morphologies are not separated by straight lines (Fig. 2).

The size prediction diagram for spherical micelles reported in Figure 3 shows how the hydrodynamic size varies with block copolymer composition, covering a radius range between 4.5 and 12 nm, using variations in the PEO and PCL block molar masses. The same plots can be generated to predict the cross-sectional radius of cylindrical micelles, and the thickness of vesicles and flat bilayers (not reported here). The sizes calculated by SCF follow the scaling behavior predicted by Zhulina et al.[15] for star-like micelles ($R_H \sim m^{3/5}$, with m indicating the number of CL units).

The concentration profiles as a function of the distance from the center (r) of the morphology are given in Figure 4. These profiles illustrate the volume fraction of the various components from the inside of the morphologies toward the bulk solvent. Such density profiles have been used to quantify the core and corona sizes and the solvent fraction in both the core and the corona.

Analysis of the Self-Assembled Structures

Following the SCF predictions reported in the phase diagrams, we synthesized three different copolymers, each supposed to assemble into a different morphology, spherical micelles (Me-EO_{45}-b-CL_{12}), cylindrical micelles (Me-EO_{45}-b-CL_{35}), and bilayers (Me-EO_{45}-b-CL_{87}). The copolymers were characterized by NMR and SEC, and their assemblies in

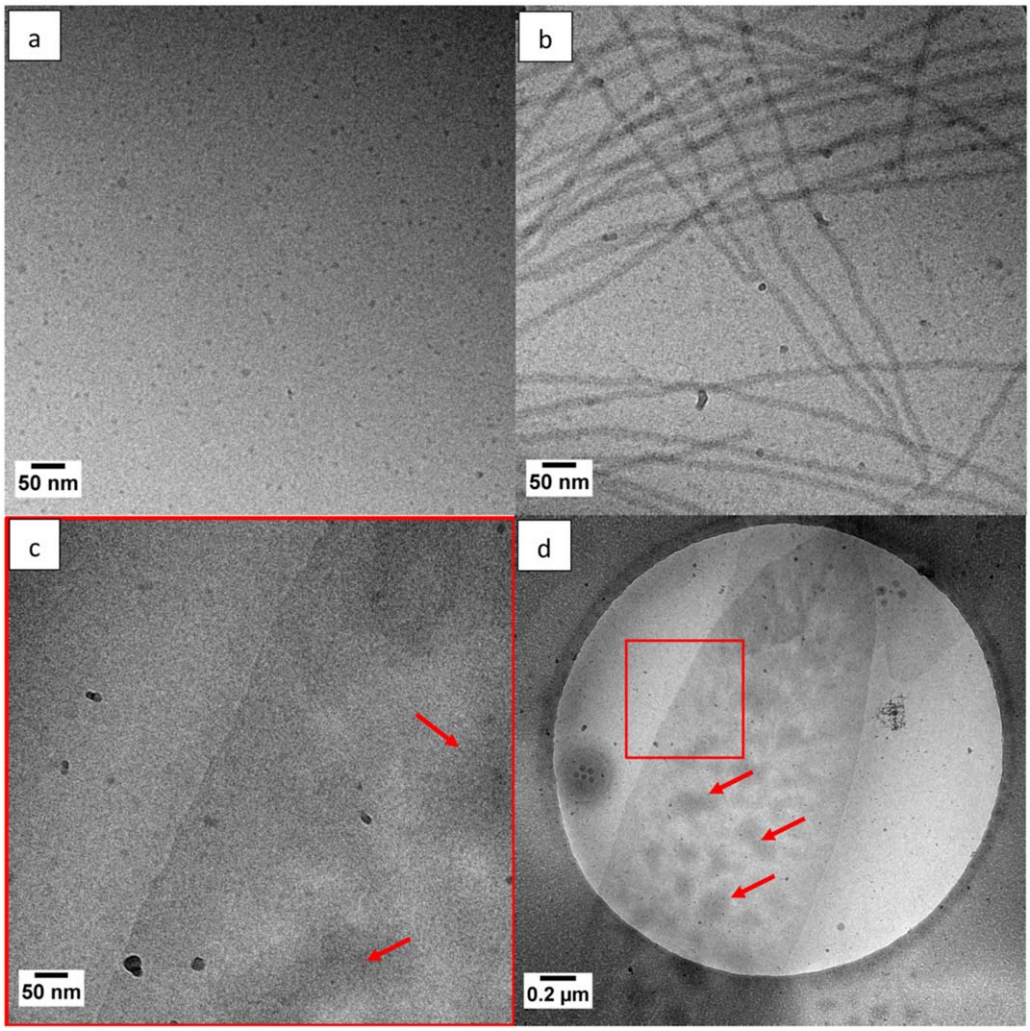

FIGURE 5 Cryo-TEM images of (a) EO_{45}-b-CL_{12}; images show spherical micelles with a radius of 4.5 ± 1 nm. (b) Me-EO_{45}-b-CL_{35}; images display cylindrical micelles with a cross sectional radius of 8 ± 1 nm surrounded by minor ice contamination. (c,d) Me-EO_{45}-b-CL_{87}; on image (c) multiple leaf shaped bilayer, the dominant observed morphology, can be seen. At high magnification (c) an edge with thickness 14 ± 9 nm can be observed. Furthermore, in image (d) centre-left a seemingly micellar packed spherical structure can be observed. Red arrows indicate some of the areas with darker contrast, attributed to the presence of crystalline domains. [Color figure can be viewed at wileyonlinelibrary.com]

water were characterized by SAXS, cryo-TEM, and MA-DLS. The results are summarized in Table 1 and details for each method are given in the Supporting Information.

Spherical Micelles from Me-EO_{45}-b-CL_{12}

The SCF results for Me-EO_{45}-b-CL_{12} copolymers show that the preferred configuration in water is spherical micelles with a core radius of 4.5 nm, a corona thickness of 4.5 nm (total $R_H = 9$ nm) and an aggregation number of $g^{SCF} = 231$ (see Supporting Information for details about the calculation of g^{SCF}). The SCF results also show the average solvent volume fraction in the core and corona to be 0.05 and 0.75, respectively. Due to the isotropy of the spherical micelle morphology, SCF essentially provides a full description of the molecular organization with makes up the self-assembled structures.

Experimentally, the spherical morphology is confirmed via the cryo-TEM [Fig. 5(a)] and SAXS (Fig. 6). A good fit of SAXS scattered intensity data was obtained using a spherical core-shell form factor.[53] The core size was measured to be 4 ± 2 nm via cryo-TEM, while both the core size and overall particle radius were determined to be 8 and 11 nm, respectively, from the SAXS data. The particles hydrodynamic radius was measured by MA-DLS, which gave a value of 9 nm. The SAXS analysis is also able to estimate the average solvent volume fraction in the coral and coronal domains. This can be evaluated via the electron length density values obtained by the fitting ($1.036 \cdot 10^{-5}$ Å^{-2} for the core, $9.855 \cdot 10^{-6}$ Å^{-2} for the shell), which resulted in values of 0.05 and 0.87, respectively (details of these calculations available in the Supporting Information). From the forward ($q \to 0$) scattered intensity value, it was possible to calculate the aggregation number $g^{SAXS} = 225$ for

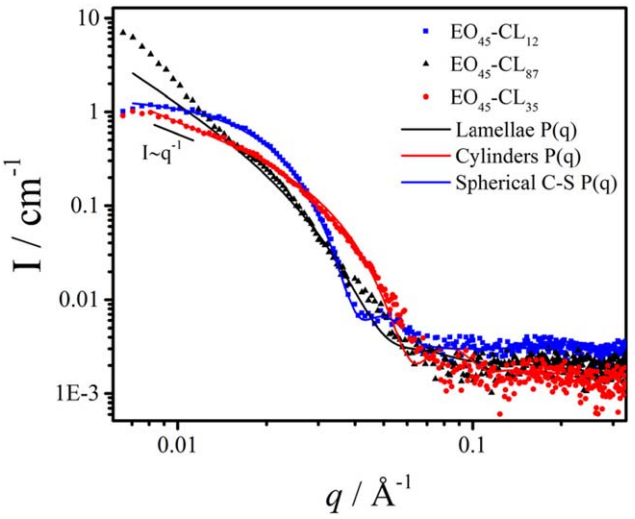

FIGURE 6 SAXS scattered intensities as function of the wave vector q for (blue squares) Me-EO_{45}-b-CL_{12}, (red dots) Me-EO_{45}-b-CL_{35} and (black triangles) Me-EO_{45}-b-CL_{87} copolymers in water at concentration of 5 mg·mL^{-1}. Fits of form factors for lamellae, cylinders, and (core + shell) spheres are plotted as the solid curves. [Color figure can be viewed at wileyonlinelibrary.com]

Me-EO_{45}-b-CL_{12} (details of these calculations available in the Supporting Information), which is in close agreement with the SCF value of 231.

Hence, the experimental data quantitatively and qualitatively agree with the theoretical SCF predictions, which validate the model and indicates that the micelles are in a low energy configuration.

Cylindrical Micelles from Me-EO_{45}-b-CL_{35}

For Me-EO_{45}-b-CL_{35} copolymers, the SCF calculations reveal the preferred configuration in water is obtained by adopting a cylindrical micelle geometry with a core radius of 8 nm and a corona size of 4 nm (total radius = 12 nm). The length of cylindrical micelles is determined by kinetic parameters which are not accounted for in the SCF simulations (in SCF the length of the cylinder is assumed to be infinite). However, if the length of the cylinders can be determined experimentally, this information combined with the SCF simulations can be used to determine the total aggregation number of the structures. The SCF average solvent volume fraction in the core and corona is 0.05 and 0.74, respectively.

The morphology of the Me-EO_{45}-b-CL_{35} copolymer assembly was again confirmed via cryo-TEM [Fig. 5(b)] and SAXS analysis. The scattered intensity profile shows the typical features associated with the presence of cylindrical objects. At low q, the scattered intensity gets proportional to q^{-1}, as expected for cylinders. The intensity $I(q)$ data were fitted to a flexible cylinder form factor[54] (Fig. 6, red curve) with cylinder cross sectional radius of 6 ± 1 nm and Kuhn length 60 nm. This indicates that the cylindrical micelles of PEO-PCL are quite flexible in solution, which is in contradiction to the cryo-TEM analysis. However, the cryo-TEM procedure involves confinement of the cylinders to a thin (usually of the order of 100–200 nm) film of water. In this regime, due to their high excluded volume, rods align to maximize their translational entropy,[55] assuming a straight configuration which may result in an apparent higher persistence length. However, the cryo-TEM analysis shows that the cylinders are not perfectly straight, but present small bending points spaced roughly 50–70 nm. This distance compares with the Kuhn length measured by SAXS.

A comparison of the experimental data with the SCF concentration profile (Fig. 4) shows that the characteristic dimensions obtained by SAXS ($P = 6 \pm 1$ nm) and cryo-TEM ($P = 8 \pm 4$ nm) correspond to the size of the dense PCL core. This can be a consequence of the low contrast of the highly hydrated PEO coronal region.

Bilayers from Me-EO_{45}-b-CL_{87}

The SCF simulations for Me-EO_{45}-b-CL_{87} copolymers show that the preferred morphology in water is bilayer with a core thickness 16 nm and corona thickness of 6 nm (total thickness $H = 28$ nm). In solution, bilayers are known to adopt either flat, curved, or closed spherical (vesicles) morphologies.

The SAXS scattered intensity data (Fig. 6, black triangles) were modeled using a flat lamellae form factor[56] (Fig. 6, black curve), resulting in a thickness of 12 ± 2 nm. At $q \approx 2 \cdot 10^{-3}$ $Å^{-1}$ (Fig. 6). It is interesting to note the contribution of small aggregates with sizes in the order of few tens of nm. These aggregates can be kinetic products originating from the preparation procedure. At lower q values ($q < 10^{-3}$ $Å^{-1}$, Fig. 6), the intensity deviates from the typical behavior expected for flat objects ($I \sim q^{-2}$). This is due to the contribution of the structure factor, indicating the tendency of the lamellae to form stacks.

The cryo-TEM image shows the presence of both flat/curved bilayers [Fig. 5(c,d)] and vesicles (Supporting Information Fig. S7). The flat bilayers have a membrane thickness of 14 ± 9 nm and are much larger and observed much more frequently than the vesicles. This explains the good fit of the SAXS data to the flat bilayer model as they will dominate the scattering profile.

According to theory, the vesicles configuration is favored over the planar as long as the number of polymers per surface area is smaller in the inner layer than in the outer one.[57,58] In this case, the curvature reduces the steric repulsion between the lyophilic chains, and no edges are present.

Me-EO_{45}-b-CL_{87} forms mostly leaf shape bilayer due to the presence of crystalline domains, which prevent the bending of the structure into vesicles. The presence of crystalline material was investigated in solution via X-ray diffraction (XRD) and on a freeze-dried sample via differential scanning calorimetry (DSC). The XRD pattern (Supporting Information Fig. S3) shows diffraction peaks corresponding to a d-spacing of 4.2 and 3.8 nm, which is consistent with PCL crystals.[59] The DSC

thermogram shows a clear melting peak with maximum at 56 °C (Supporting Information Fig. S4) associated with the PCL crystals melting.[60] The morphology of our leaf-shaped bilayers also link to those observed for PEO-PCL single crystals prepared in dilute solutions of *n*-hexanol.[36,61] From the cryo-TEM image of the lamellar structures, it is also possible to identify a zone with higher contrast, which can be attributed to the crystalline domains. The data suggest that a competition between self-assembly (formation of vesicles) and crystallization (formation of flat bilayers) can arise during the gradual solvent switch from acetone to water, which will be discussed in detail in a following publication.

Finally, it seems that also for the leaf-shaped bilayers, SAXS and cryo-TEM provide a measurement of the dense PCL core size, similarly to the case of worm-like micelles, as appears from the comparison with the SCF concentration profiles (Fig. 4).

CONCLUSIONS

In this work, we have shown that SCF computations enable reliable predictions for the self-assembly behavior of block copolymers in a selective solvent. These predictions, in the form of quantitative phase and size diagrams, allow the *a priori* design of copolymers into supramolecular architectures with tailored size and morphology. This represents a huge advantage, as time consuming experimental trial and error can be avoided. The SCF predictions also provide a framework to understand whether a self-assembled structure is in thermodynamic equilibrium or not. This is extremely important, as out of equilibrium structures can be unstable over time.

PEO-PCL block copolymers corresponding to the ones used for the SCF predictions have been synthesized with a one pot solvent free and metal free method reported previously, to have high biocompatibility and control over molar mass (dispersity). The self-assembly behavior of these copolymers was investigated by means of a wide range of complementary characterization methods, that is, SAXS, cryo-TEM, and MA-DLS.

The theoretically predicted and measured morphology and size of self-assembled structures copolymers are in agreement. It has been shown that it is possible to obtain spherical nanoparticles with hydrodynamic radii ranging from 5 to 17 nm using block copolymers obtained by PEO initiators with different average molar mass, and we provided a size diagram which enables particle size predictions as a function of the copolymer composition.

We observed that crystallization and self-assembly can simultaneously occur for Me-EO_{45}-b-CL_{87} copolymer. This shows that the possibility of crystallization must be taken into account to control the self-assembly process of copolymers containing semi-crystalline polymeric units.

The SCF computations have been compared with experimental and literature data of morphology showing good agreement. This shows that SCF is a very powerful tool for both making reliable predictions about the equilibrium properties and guiding the interpretation of experimental data concerning self-assembled block copolymers structures.

The predict-synthesize-characterize platform proposed here represents a toolbox for designing and making on-demand self-assembled structures for a wide range of applications, particularly for drug delivery and *in vivo* bio imaging.

ACKNOWLEDGMENTS

The authors thank J. G. J. L. Lebouille, A. V. Petukhov, F. S. Bates, and J. S. Pedersen for fruitful discussions, C. Guilbert for the help with the preliminary SAXS measurements, and D. J. G. P. van Osch for performing the density measurements.

REFERENCES AND NOTES

1 G. J. Fleer, M. A. Cohen Stuart, J. M. H. M. Scheutjens, T. Cosgrove, B. Vincent, *Polymers at Interfaces*; Springer: Netherlands, **1998**.

2 Y. Mai, A. Eisenberg, *Chem. Soc. Rev.* **2012**, *41*, 5969.

3 S. J. Holder, N. A. J. M. Sommerdijk, *Polym. Chem.* **2011**, *2*, 1018.

4 B. E. Mckenzie, H. Friedrich, M. J. M. Wirix, J. F. D. Visser, O. R. Monaghan, P. H. H. Bomans, F. Nudelman, S. J. Holder, N. A. J. M. Sommerdijk, *Angew. Chem.* **2015**, *127*, 2487.

5 M. Karayianni, S. Pispas, In *Fluorescence Studies of Polymer Containing Systems*; Springer International Publishing: Switzerland, **2016**; pp 27–64.

6 R. Haag, *Angew. Chem. Int. Ed. Engl.* **2004**, *42*, 278.

7 P. Alexandridis, *Curr. Opin. Colloid Interf. Sci.* **1996**, *1*, 490.

8 J. Chen, F. Wang, Q. Liu, J. Du, *Chem. Commun.* **2014**, *50*, 14482.

9 T. Wang, J. Jiang, Y. Xiao, Y. Zou, J. Gao, J. Du, *RSC Adv.* **2015**, *5*, 55602.

10 H. Otsuka, Y. Nagasaki, K. Kataoka, *Curr. Opin. Colloid Interf. Sci.* **2001**, *6*, 3.

11 A. H. Gröschel, A. H. E. Müller, *Nanoscale.* **2015**, *7*, 11841.

12 Y. Yu, L. Zhang, A. Eisenberg, *Macromolecules* **1998**, *31*, 1144.

13 H. Cui, Z. Chen, S. Zhong, K. L. Wooley, D. J. Pochan, *Science* **2007**, *317*, 647.

14 J. N. Israelachvili, D. J. Mitchell, W. B. Ninham, *J. Chem. Soc. Faraday Trans. 2 Mol. Chem. Phys.* **1975**, 1525.

15 E. B. Zhulina, M. Adam, I. Larue, S. S. Sheiko, M. Rubinstein, *Macromolecules* **2005**, *38*, 5330.

16 R. Nagarajan, E. Ruckenstein, *Langmuir* **1991**, *7*, 3, 2934.

17 E. B. Zhulina, O. V. Borisov, *Macromolecules* **2012**, *45*, 4429.

18 P. N. Hurter, J. M. H. M. Scheutjens, T. A. Hatton, *Macromolecules* **1993**, *26*, 5592.

19 T. Lindvig, M. L. Michelsen, G. M. Kontogeorgis, *Fluid Phase Equilib.* **2002**, *203*, 247.

20 N. Shuld, B. A. Wolf, In *Polymer Handbook*; Wiley: New York, **2003**.

21 P. J. Flory, *Principles of Polymer Chemistry*; Cornell University Press: Ithaca, NY, **1953**.

22 J. Lyklema, *Fundamentals of Interface and Colloid Science*; Elsevier B.V.: Amsterdam, **2005**; Vol. *V*.

23 D. B. Shenoy, M. M. Amiji, *Int. J. Pharm.* **2005**, *293*, 261.

24 Z. Zhu, C. Xiong, L. Zhang, X. Deng, *J. Polym. Sci. Part A-Polymer Chem.* **1997**, *35*, 709.

25 A. Ianiro, I. Jimenez-Pardo, A. C. C. Esteves, R. Tuinier, *J. Polym. Sci. Part A-Polymer Chem.* **2016**, *54*, 2992.

26 C. J. Drummond, C. Fong, *Curr. Opin. Colloid Interface Sci.* **1999**, *4*, 449.

27 J. G. J. L. Lebouille, L. F. W. Vleugels, A. A. Dias, A. M. F. Leermakers, M. A. Cohen Stuart, R. Tuinier, *Eur. Phys. J. E.* **2013**, *36*,

28 A. S. Mikhail, C. Allen, *Biomacromolecules* **2010**, *11*, 1273.

29 S. Schöttler, G. Becker, S. Winzen, T. Steinbach, K. Mohr, K. Landfester, V. Mailänder, F. R. Wurm, *Nat. Nanotechnol.* **2016**, *11*, 372.

30 S. Cai, K. Vijayan, D. Cheng, E. M. Lima, D. E. Discher, *Pharm. Res.* **2007**, *24*, 2099.

31 Y. Geng, P. Dalhaimer, S. Cai, R. Tsai, M. Tewari, T. Minko, D. E. Discher, *Nat. Nanotechnol.* **2007**, *2*, 249.

32 Y. Kim, P. Dalhaimer, D. A. Christian, D. E. Discher, *Nanotechnology* **2005**, *16*, S484.

33 D. J. Adams, C. Kitchen, S. Adams, S. Furzeland, D. Atkins, P. Schuetz, C. M. Fernyhough, N. Tzokova, J. A. Ryan, M. F. Butler, *Soft Matter.* **2009**, *5*, 3086.

34 Z. Du, J. Xu, Z. Fan, *Macromolecules* **2007**, *40*, 7633.

35 P. Vangeyte, S. Gautier, R. Jérome, *Colloids Surfaces A Physicochem. Eng. Asp.* **2004**, *242*, 203.

36 J. Sun, X. Chen, C. He, X. Jing, *Macromolecules* **2006**, *39*, 3717.

37 W. Qi, P. P. Ghoroghchian, G. Li, A. Hammer, M. J. Therien, *Nanoscale* **2013**, *5*, 10908.

38 B. Du, A. Mei, K. Yin, Q. Zhang, J. Xu, Z. Fan, *Macromolecules* **2009**, *42*, 8477.

39 Z. Zhou, Z. Li, Y. Ren, M. A. Hillmyer, T. P. Lodge, *J. Am. Chem. Soc.* **2003**, *125*, 10182.

40 W. Ding, S. Lin, J. Lin, L. Zhang, *J. Phys. Chem. B.* **2008**, *112*, 776.

41 S. Lin, X. He, Y. Li, J. Lin, T. Nose, *J. Phys. Chem. B.* **2009**, *113*, 13926.

42 E. Konishcheva, D. Häussinger, S. Lörcher, W. Meier, *Eur. Polym. J.* **2016**, *83*, 300.

43 J. G. J. L. Lebouille, R. Tuinier, L. F. W. Vleugels, M. A. Cohen Stuart, F. A. M. Leermakers, *Soft Matter.* **2013**, *9*, 7515.

44 E. E. Dormidontova, *Macromolecules* **2002**, *35*, 987.

45 T. Shikata, M. Okuzono, N. Sugimoto, *Macromolecules* **2013**, *46*, 1956.

46 K. Ragaert, G. Maeyaert, M. Ci, L. Cardon, *J. Mater. Sci. Eng.* **2014**, *3*, 3.

47 J. M. H. M. Scheutjens, G. J. Fleer, M. A. Cohen Stuart, *Colloids Surf.* **1986**, *21*, 285.

48 S. Choi, F. S. Bates, T. P. Lodge, *Macromolecules* **2011**, *44*, 3594.

49 J. Lu, F. S. Bates, T. P. Lodge, *Macromolecules* **2015**, *48*, 2667.

50 S. Choi, T. P. Lodge, F. S. Bates, *Phys. Rev. Lett.* **2010**, *104*, 47802.

51 D. B. Wright, J. P. Patterson, N. C. Gianneschi, C. Chassenieux, O. Colombani, G. H. Road, L. Jolla, S. Diego, O. Messiaen, *Polym. Chem.* **2016**, *7*, 1577.

52 H. Fessi, A. F. Puisieux, J. P. Devissaguet, N. Ammoury, S. Benita, *Int. J. Pharm.* **1989**, *55*, 1.

53 A. Fournet, G. Guinier, *Small-Angle Scattering of X-Rays*; Wiley: New York, **1955**.

54 J. S. Pedersen, P. Schurtenberger, *Macromolecules* **1996**, *29*, 7602.

55 D. Frenkel, *Nat. Mater.* **2015**, *14*, 9.

56 F. Nallet, R. Laversanne, D. Roux, *J. Phys. II.* **1993**, *3*, 487.

57 H. T. Jung, B. Coldren, J. A. Zasadzinski, D. J. Iampietro, E. W. Kaler, *Proc. Natl. Acad. Sci.* **2001**, *98*, 1353.

58 Z. Wang, *Macromolecules* **1992**, *25*, 3702.

59 A. Baji, S. Wong, T. Liu, T. Li, T. S. Srivatsan, *J. Biomed. Mater. Res. Part B Appl. Biomater.* **2006**, 343.

60 Z. Wei, F. Yu, G. Chen, C. Qu, P. Wang, W. Zhang, J. Liang, M. Qi, L. Liu, *J. Appl. Polym. Sci.* **2009**, *114*, 1133.

61 R. M. Van Horn, J. X. Zheng, H. Sun, M. Hsiao, W. Zhang, X. Dong, J. Xu, E. L. Thomas, B. Lotz, S. Z. D. Cheng, *Macromolecules* **2010**, *43*, 6113.